

Supplementary Methods and Results
Empowering the crowd: Feasible strategies
to minimize the spread of COVID-19
in informal settlements

Alberto Pascual-García^{(1,*),} Jordan Klein⁽²⁾, Jennifer Villers^(3,^),
Eduard Campillo-Funollet^(4,^), Chamsy Sarkis⁽⁵⁾

February 8, 2021

(1) Institute of Integrative Biology. ETH-Zürich. Zürich, Switzerland.

(2) Office of Population Research. Princeton University. Princeton, NJ, USA.

(3) Princeton Environmental Institute. Princeton University. Princeton, NJ, USA.

(4) Genome Damage and Stability Centre. University of Sussex. Brighton, United Kingdom.

(5) Pax Syriana Foundation. Valetta, Malta.

(^) Equal contribution.

(*) correspondence: alberto.pascual@env.ethz.ch

Parameterization of the model

Derivation of fixed parameters (Main Table ??)

To estimate the latent period ($1/\delta_E$), we calculated the difference between randomly generated incubation ($1/\delta_E + 1/\delta_P$) and presymptomatic ($1/\delta_P$) periods. We estimated the presymptomatic period using results reported by He et al. [1] and found they best fit a Gompertz distribution with a mean of 2.3 days (95% CI: 0.8-3.0). Since a correction of these by Ashcroft et al. [2] suggests they significantly underestimate the presymptomatic period's upper bound, we estimated that the true presymptomatic period follows a Gaussian distribution around the mean (95% CI: 0.8-3.8). However, this presymptomatic period distribution implies a non-negligible probability of a negative latent period. To correct this discrepancy, we assumed a minimum latent period of .5 days [3]. Time from symptom onset to death in critical cases ($1/\alpha$) is estimated using time from symptom onset to ICU admission in Wang et al [4].

Derivation of transmissibility parameters (Main Table ??)

ρ_{HI} calculated manually from van Kampen et al.[5] by the ratio of viral culture positive test rate in hospitalized patients 7-16 days since start of symptoms to positive test rate in patients 0-6 days since start of symptoms.

$$\beta_A = \beta_I \rho_{AI} \quad (1)$$

$$\beta_H = \beta_I \rho_{HI} \quad (2)$$

$$\frac{AUC_P}{(1 - AUC_P)} = \frac{\frac{\beta_P}{\delta_P}}{\frac{\beta_I}{\gamma_I} + \frac{\beta_H}{\gamma_H}} \quad (3)$$

$$\beta_I \gamma_H + \beta_H \gamma_I = \frac{\beta_P \gamma_I \gamma_H (1 - AUC_P)}{AUC_P \delta_P} \quad (4)$$

$$\beta_I \gamma_H + \beta_I \rho_{HI} \gamma_I = \frac{\beta_P \gamma_I \gamma_H (1 - AUC_P)}{AUC_P \delta_P} \quad (5)$$

$$\beta_I = \frac{\beta_P \gamma_I \gamma_H (1 - AUC_P)}{AUC_P \delta_P (\gamma_H + \rho_{HI} \gamma_I)} \quad (6)$$

$$\beta_A = \frac{\rho_{AI} \beta_P \gamma_I \gamma_H (1 - AUC_P)}{AUC_P \delta_P (\gamma_H + \rho_{HI} \gamma_I)} \quad (7)$$

$$\beta_H = \frac{\rho_{HI} \beta_P \gamma_I \gamma_H (1 - AUC_P)}{AUC_P \delta_P (\gamma_H + \rho_{HI} \gamma_I)} \quad (8)$$

Population structure of demographic-classes derivation (Main Table ??)

In April, 2020, 40.7% of the population in informal IDP camps in Northern Syria was aged 0-12, 53.4% aged 13-50, and 5.9% aged 51+ [6]. To estimate the proportion of each age group with comorbidities, we calculated the weighted average age-specific comorbidity prevalence of the 4 most common comorbidities in the Syrian refugee populations in Jordan and Lebanon: hypertension, cardiovascular disease, diabetes, and chronic respiratory disease [7, 8]. We standardized these weighted averages to the age structure of IDPs in Northern Syria and estimated that 11.7% of people aged 13-50 have comorbidities, while 62.9% of people aged 51+ have comorbidities.

We estimated the fractions of symptomatic cases in children aged <13 that would become severe and critical from the fractions of symptomatic cases in children aged <11 that were severe and critical in China [9]. We estimated the class-specific fractions of symptomatic cases in adults that would become severe and critical using the age and

comorbidity-specific fractions of symptomatic cases with known outcomes that required hospitalization, without and with ICU admission, respectively in the United States [10]. To account for poorer health among Syrian adults compared to their similarly aged peers in developed countries, estimates for US adults aged 19-64 were used for Syrian adults aged 13-50, while estimates for US adults aged 65+ were used for Syrian adults aged 51+.

Derivation of epidemiology severity parameters

Derivation of the transmissivity parameter τ

Estimation of the Next Generation Matrix

In the following, to simplify the notation we define $\kappa_i = (l_i\gamma_I + h_i\eta + g_i\alpha)$. To estimate the probability of infection if there is a contact between a susceptible and an infected individual (parameter τ) we proceed as follows [11, 12, 13]. We start by considering the subsystem containing the infected population:

$$\dot{E}_i = \lambda_i S_i - \delta_E E_i \quad (9)$$

$$\dot{P}_i = \delta_E E_i - \delta_P P_i \quad (10)$$

$$\dot{A}_i = (1 - f)\delta_P P_i - \gamma_A A_i \quad (11)$$

$$\dot{I}_i = f\delta_P P_i - \kappa_i I_i \quad (12)$$

$$\dot{H}_i = h_i\eta I_i - \gamma_H H_i. \quad (13)$$

For the sake of simplifying the notation, let us consider the following ordering of the variables in the vector $x = (E_1, \dots, E_M, P_1, \dots, P_M, A_1, \dots, A_M, I_1, \dots, I_M, H_1, \dots, H_M)$, with M the number of population classes. We are interested in the parameterization of the null model, which will serve as a baseline to estimate the parameter τ , which is initially unknown, but does not change when interventions are introduced. Considering the contacts matrix for the null model (Eq. ?? in Main Text), the rate of exposure becomes

$$\lambda_i = \frac{\tau}{N} \sum_{j=1}^M c_i (\beta_P P_j + \beta_A A_j + \beta_I I_j + \beta_H H_j). \quad (14)$$

In the following, we use bold symbols for vectors and matrices, and the symbols \odot and \oslash for the element-wise multiplication and division, respectively. Following this notation, the linearized system can be written in the form $\dot{x} = (\mathbf{T} + \Sigma)x$, where:

$$\mathbf{T} = \tau \begin{bmatrix} \mathbf{0} & \Theta_P & \Theta_A & \Theta_I & \Theta_H \\ \mathbf{0} & \mathbf{0} & \mathbf{0} & \mathbf{0} & \mathbf{0} \\ \mathbf{0} & \mathbf{0} & \mathbf{0} & \mathbf{0} & \mathbf{0} \\ \mathbf{0} & \mathbf{0} & \mathbf{0} & \mathbf{0} & \mathbf{0} \\ \mathbf{0} & \mathbf{0} & \mathbf{0} & \mathbf{0} & \mathbf{0} \end{bmatrix} \quad (15)$$

is the transmission matrix, with $\Theta_X = \beta_X \text{diag}(\mathbf{p} \odot \mathbf{c})\mathbf{U}$, $\mathbf{p} = \mathbf{N}/N$, \mathbf{U} is the all-ones matrix of size M , and β_X the infectiousness of compartment X relative to the presymptomatic compartment (see Main Text for details). The transition matrix is

$$\Sigma = \begin{bmatrix} -\delta_E \mathbf{I} & \mathbf{0} & \mathbf{0} & \mathbf{0} & \mathbf{0} \\ \delta_E \mathbf{I} & -\delta_P \mathbf{I} & \mathbf{0} & \mathbf{0} & \mathbf{0} \\ \mathbf{0} & (1-f)\delta_P \mathbf{I} & -\gamma_A \mathbf{I} & \mathbf{0} & \mathbf{0} \\ \mathbf{0} & f\delta_P \mathbf{I} & \mathbf{0} & -\text{diag}(\kappa) \mathbf{I} & \mathbf{0} \\ \mathbf{0} & \mathbf{0} & \mathbf{0} & \eta \text{diag}(\mathbf{h}) \mathbf{I} & -\gamma_H \mathbf{I} \end{bmatrix} \quad (16)$$

Where \mathbf{I} and $\mathbf{0}$ are the identity and null matrices of size M , and $\kappa = l\gamma_I + h\eta + g\alpha$. We next compute the inverse of the transition matrix

$$\Sigma^{-1} = \begin{bmatrix} -\frac{1}{\delta_E} \mathbf{I} & \mathbf{0} & \mathbf{0} & \mathbf{0} & \mathbf{0} \\ -\frac{1}{\delta_P} \mathbf{I} & -\frac{1}{\delta_P} \mathbf{I} & \mathbf{0} & \mathbf{0} & \mathbf{0} \\ -\frac{(1-f)}{\gamma_A} \mathbf{I} & -\frac{(1-f)}{\gamma_A} \mathbf{I} & -\frac{1}{\gamma_A} \mathbf{I} & \mathbf{0} & \mathbf{0} \\ -f \text{diag}(\boldsymbol{\kappa}^{-1}) \mathbf{I} & -f \text{diag}(\boldsymbol{\kappa}^{-1}) \mathbf{I} & \mathbf{0} & -\text{diag}(\boldsymbol{\kappa}^{-1}) \mathbf{I} & \mathbf{0} \\ -\frac{f\eta}{\gamma_H} \text{diag}(\mathbf{h} \otimes \boldsymbol{\kappa}) \mathbf{I} & -\frac{f\eta}{\gamma_H} \text{diag}(\mathbf{h} \otimes \boldsymbol{\kappa}) \mathbf{I} & \mathbf{0} & -\frac{\eta}{\gamma_H} \text{diag}(\mathbf{h} \otimes \boldsymbol{\kappa}) \mathbf{I} & -\frac{1}{\gamma_H} \mathbf{I} \end{bmatrix} \quad (17)$$

The NGM with large domain can now be found by $\mathbf{K}_L = -T\Sigma^{-1}$. However, since we know that each individual who gets infected becomes exposed (E compartment), we focus on the NGM with small domain, \mathbf{K}_S , which only consists of the E compartment [14]. We do this by removing the rows that correspond to the other compartments from T and the columns from Σ^{-1} . We then find:

$$\mathbf{K}_S = \tau \left[\frac{1}{\delta_P} \Theta_P + \frac{(1-f)}{\gamma_A} \Theta_A + f \text{diag}(\mathbf{h}^{-1}) \Theta_I + \frac{f\eta}{\gamma_H} \text{diag}(\mathbf{h} \otimes \boldsymbol{\kappa}) \Theta_H \right]. \quad (18)$$

The reproduction number is related to the dominant eigenvalue of \mathbf{K}_S , i.e. $R_0 = |\lambda_1|$, and τ is estimated from the dominant eigenvalue of $\tilde{K}_S = K_S/\tau$. Considering the null model parameters $(\tilde{\lambda}_1^0)$, we have the expression:

$$\tau = \frac{R_0}{|\tilde{\lambda}_1^0|}. \quad (19)$$

Parameterization of the interventions

Safety zone (see Main Text)

To account for higher likelihood of interaction with members of the classes staying in the same zone compared to the null model, the proportion N_i/N of individuals of class i in the null model becomes N_i/N_X with N_X the total number of individuals in zone $X = \{o, g\}$. Following the main text, our equations for the redistribution of contacts compared to the null model are:

$$m_{ij} = \frac{\xi \rho c_{\text{visit}}}{c_i} \frac{N_i}{N_Y} \frac{N}{N_i} = \frac{\xi N \rho c_{\text{visit}}}{c_i N_Y} \quad (i, j \text{ in different zones } i \in X \text{ and } j \in Y) \quad (20)$$

$$m_{ij} = \frac{(1 - \rho c_{\text{visit}})}{c_i} \frac{N_i}{N_X} \frac{N}{N_i} = \frac{N(1 - \rho c_{\text{visit}})}{c_i N_X} \quad (i, j \text{ in same zone } X) \quad (21)$$

If c_{visit} is large enough ($c_{\text{visit}} \approx 15$ contacts per day), ρ should saturate, because every member of the orange zone would eventually visit the buffer zone, following the expression:

$$\rho = \begin{cases} 1 & \text{if } i \in g \\ f_{o,\text{visit}} \left(1 - \Theta(f_{o,\text{visit}} - 1) \frac{f_{o,\text{visit}} - 1}{f_{o,\text{visit}}} \right) & \text{if } i \in o \end{cases} \quad (22)$$

with the Heaviside function $\Theta(f_{o,\text{visit}} - 1) = 1$ if $f_{o,\text{visit}} \geq 1$. We chose values well below this saturation threshold (a maximum of 10 contacts per week, i.e. 1.42 contacts per day, see Main Fig. ??).

Table 1: **Fraction of population in each zone by safety zone scenario and behaviour-class.** Behaviour-classes that are not considered in a given scenario have a proportion equal to zero.

Scenario	Age 1, orange	Age 1, green	Age 2 no comorbidities, orange	Age 2 no comorbidities, green	Age 2 comorbidities, orange	Age 2 comorbidities, green	Age 3 no comorbidities, green	Age 3 comorbidities, green
Only age 3 in green zone	.407	0	.471	0	.0626	0	.022	.0373
Age 3 + age 2 with comorbidities in green zone	.407	0	.471	0	0	.0626	.022	.0373
20% green zone capacity	.376	.0312	.424	.0469	0	.0626	.022	.0373
25% green zone capacity	.356	.0512	.394	.0769	0	.0626	.022	.0373
30% green zone capacity	.336	.0712	.364	.107	0	.0626	.022	.0373

We explore different scenarios, summarized in Table 1, for allocating members of each population class to the safety, or “green” zone, and the exposed, or “orange” zone. In one scenario, we only place individuals in age group 3 (>50) in the green zone, while in another we place all vulnerable individuals, age group 3 and age group 2 (13-50) with comorbidities, in the green zone. In 3 additional scenarios, after all vulnerable individuals are allocated to the green zone, we set the green zone’s capacity to a certain percentage of the camp’s population (20%, 25%, 30%), and allocate its remainder to non-vulnerable family members, who by necessity are either children <13 in age group 1 or healthy younger adults in age group 2. In accordance with camp managers’ expectations that many vulnerable individuals will have non-vulnerable spouses, while fewer vulnerable individuals will have young children, in these scenarios we allocate 40% of the remainder of the green zone to children and 60% of the remainder of the green zone to younger adults without comorbidities. We also consider a baseline scenario in which there is no green zone.

Supplementary figures

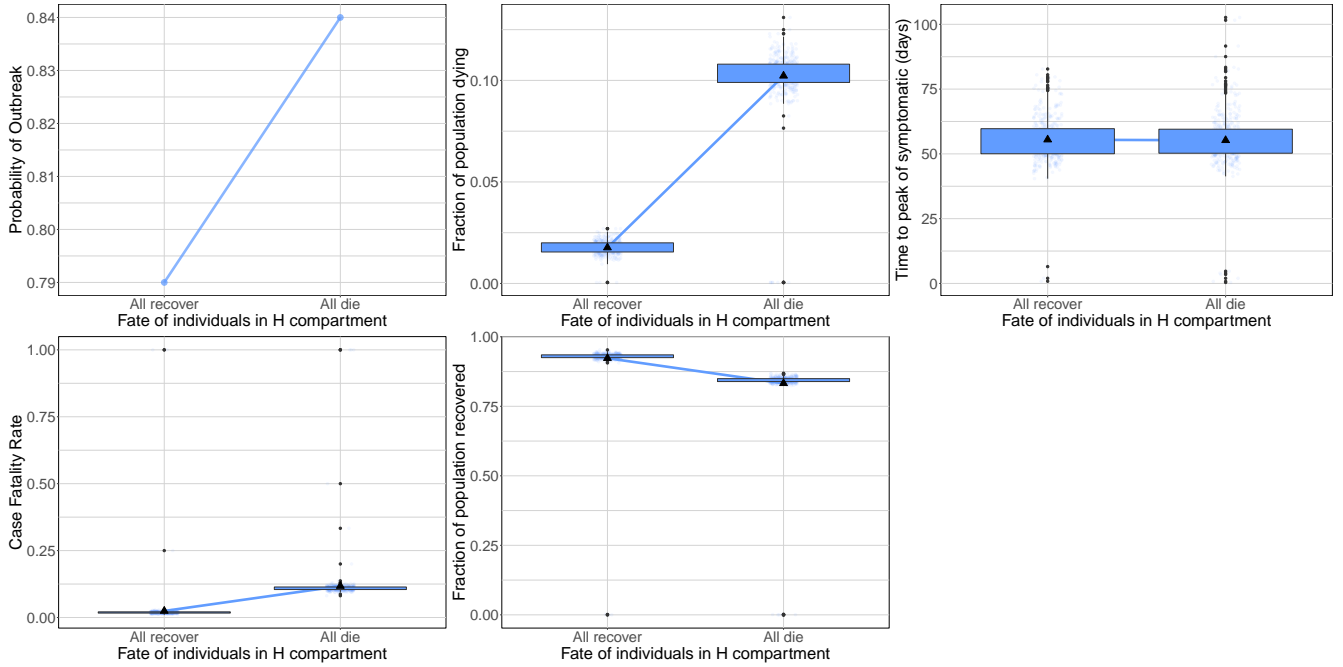


Figure 1: Outcomes when all severe (hospitalized) cases recover ($\sigma = 0$) vs when all severe (hospitalized) cases die ($\sigma = 1$). Probability of an outbreak (top left), fraction of the population dying (top middle), the probability of observing an outbreak is also necessarily higher when $\sigma = 1$.

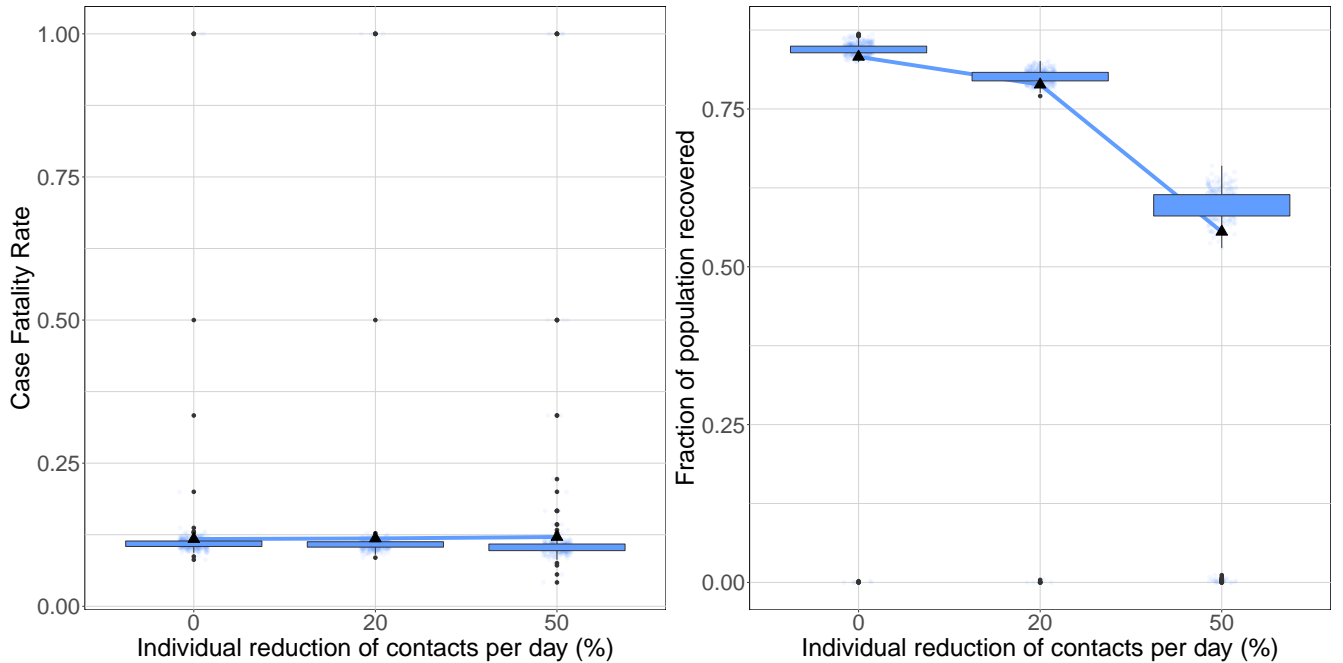


Figure 2: Self-distancing. IFR (left), and fraction of the population that recovers (right) as a function of the proportion of contacts reduced per individual per day.

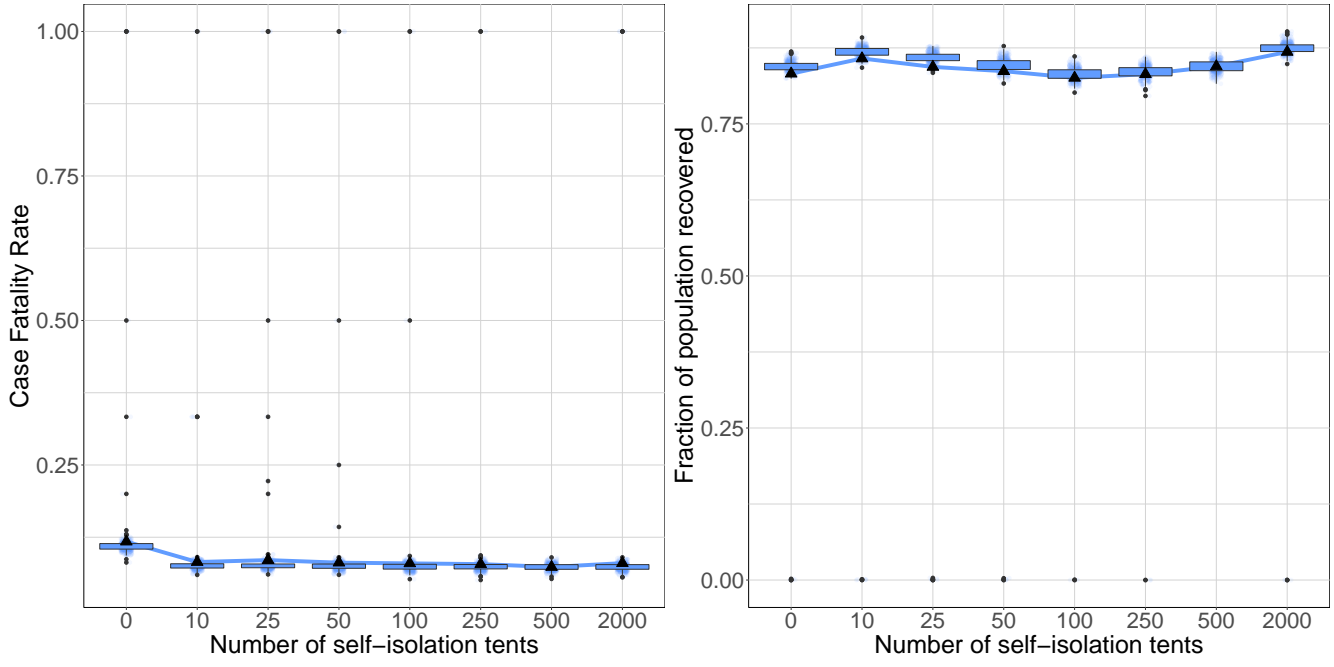


Figure 3: **Self-isolation.** IFR (left), and fraction of the population that recovers (right) as a function of the number of isolation tents available in the camp.

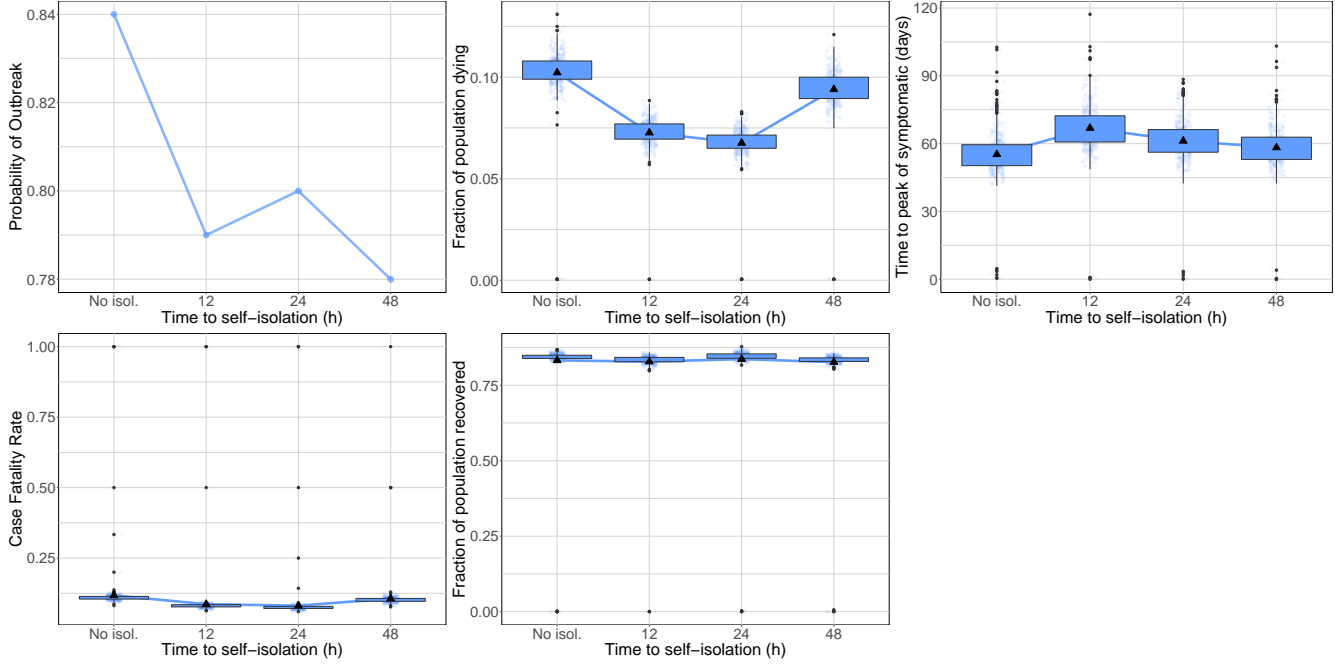


Figure 4: **Time to self-isolation.** Probability of an outbreak (top left), fraction of the population dying (top middle), time until peak symptomatic cases (top right), IFR (bottom left), and fraction of the population that recovers (bottom middle) as a function of the time that individuals require to recognize their symptoms and self-isolate.

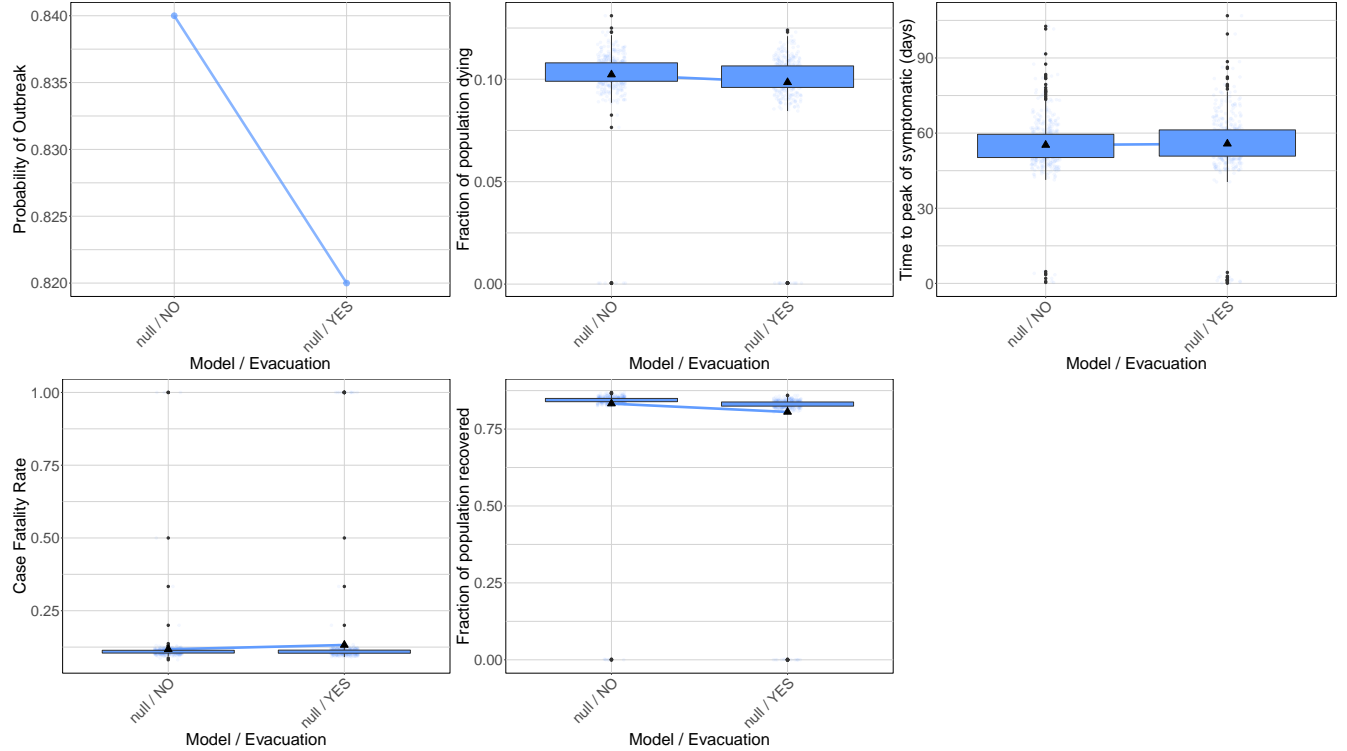


Figure 5: **Evacuation.** Probability of an outbreak (top left), fraction of the population dying (top middle), time until peak symptomatic cases (top right), IFR (bottom left), and fraction of the population that recovers (bottom middle), as a function of whether individuals requiring hospitalization are evacuated to isolation centers.

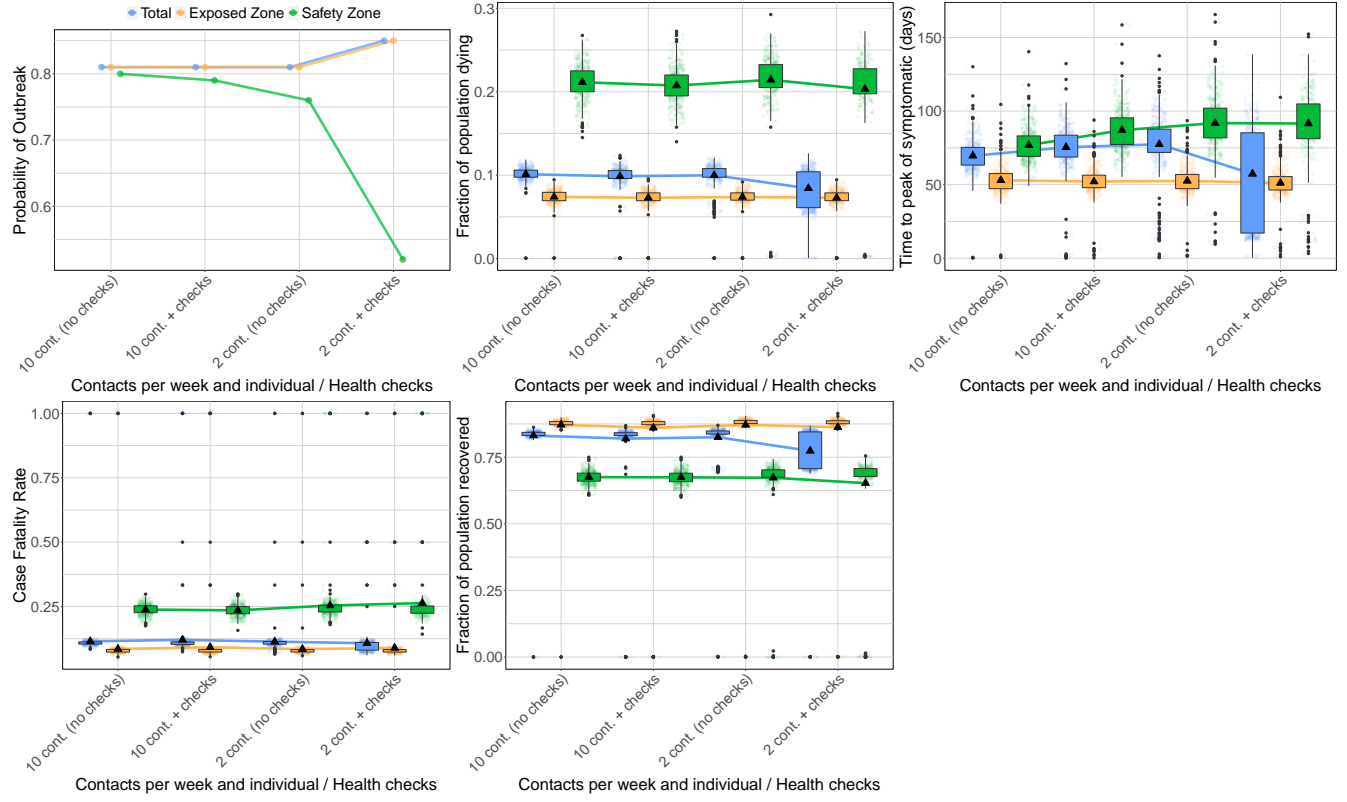


Figure 6: Health-checks in the buffer zone. Probability of an outbreak (top left), fraction of the population dying (top middle), time until peak symptomatic cases (top right), IFR (bottom left), and fraction of the population that recovers (bottom middle), as a function of whether health-checks are implemented in the buffer zone between the safety and exposed zones. Scenarios with 10 or 2 contacts in the buffer zone per person in the safety zone per week are plotted. All figures consider the scenario in which 20% of the camp's population is allocated to the safety zone.

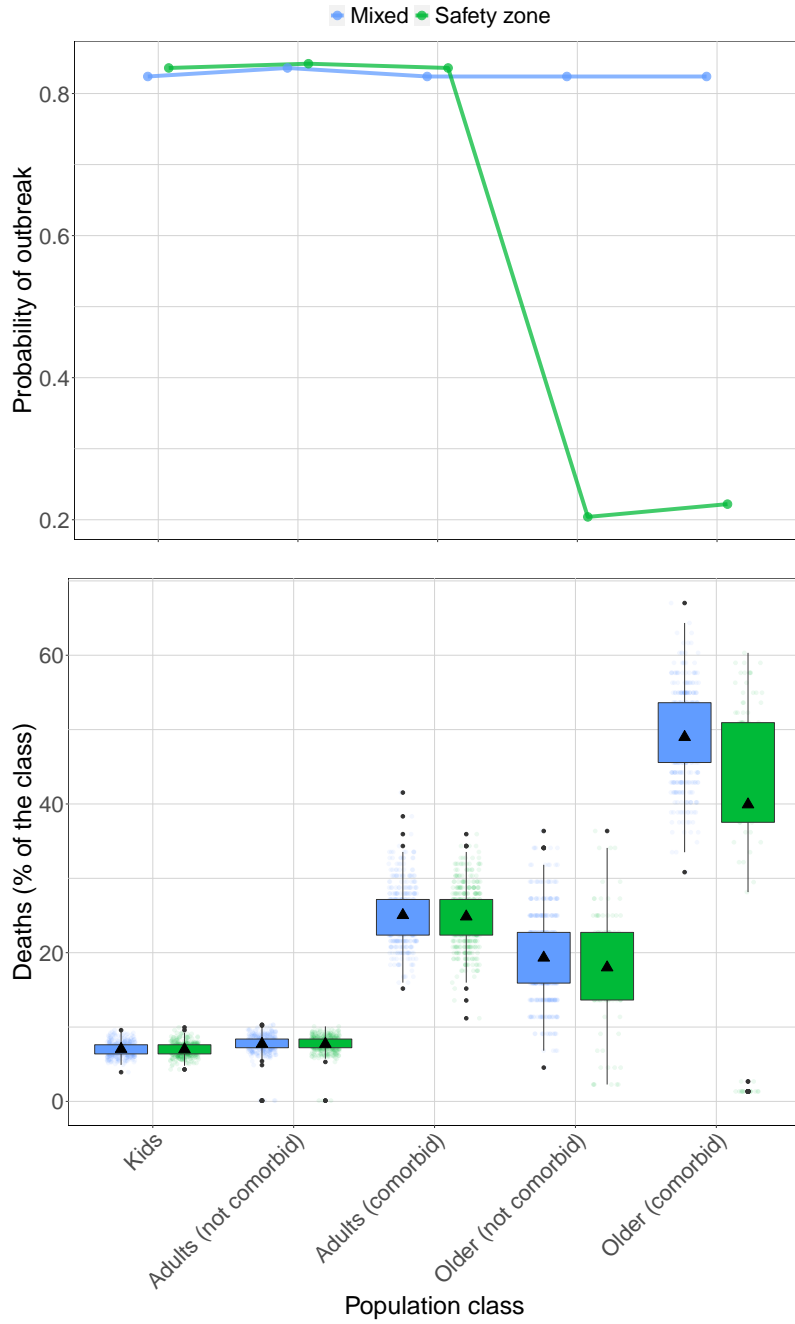


Figure 7: Effects of the safety zone on outcomes by population class. Probability of an outbreak (top), and proportion that dies in each population class (bottom) when no interventions are implemented (Mixed), compared to protection of older adults in the safety zone with 2 contacts in the buffer zone per week (Safety zone). The fraction of deaths in the safety zone for the older population is significantly lower (Kruskal-Wallis test, $p\text{-val} < 10^{-15}$).

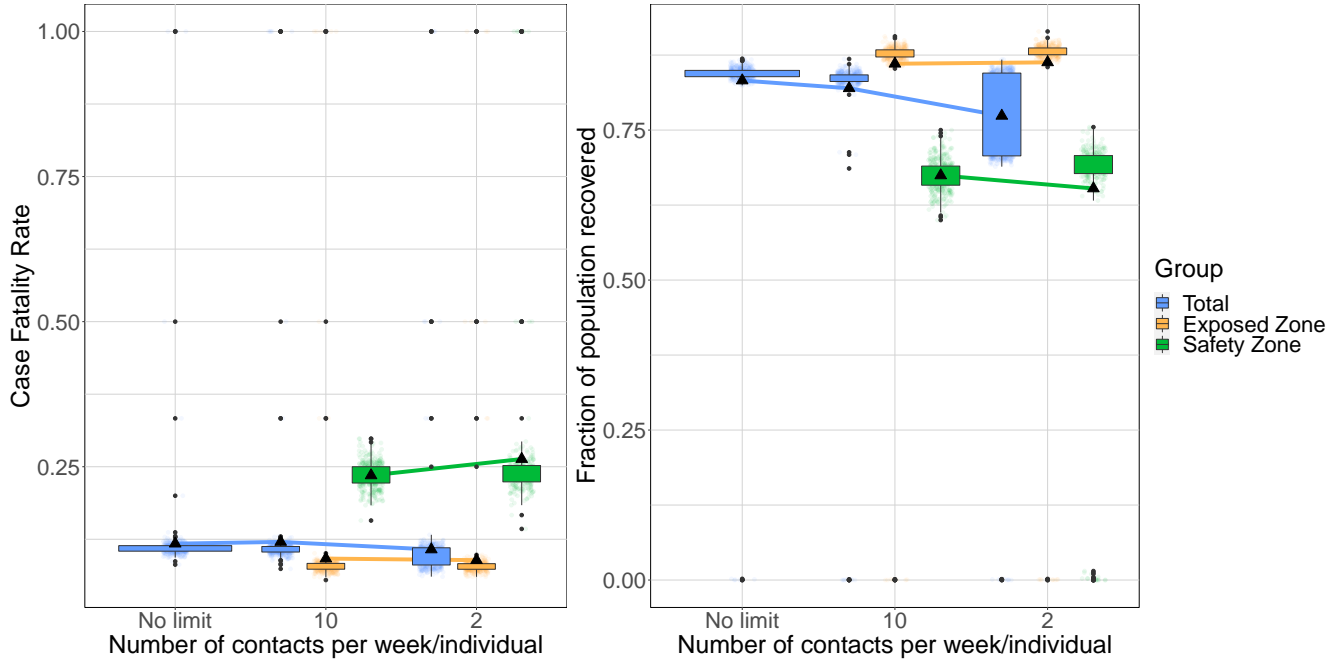


Figure 8: **Number of contacts in the buffer zone.** IFR (left), and fraction of the population that recovers (right) as a function of the number of contacts that each individual in the safety zone has in the buffer zone per week. All figures consider the scenario in which 20% of the camp's population is allocated to the safety zone.

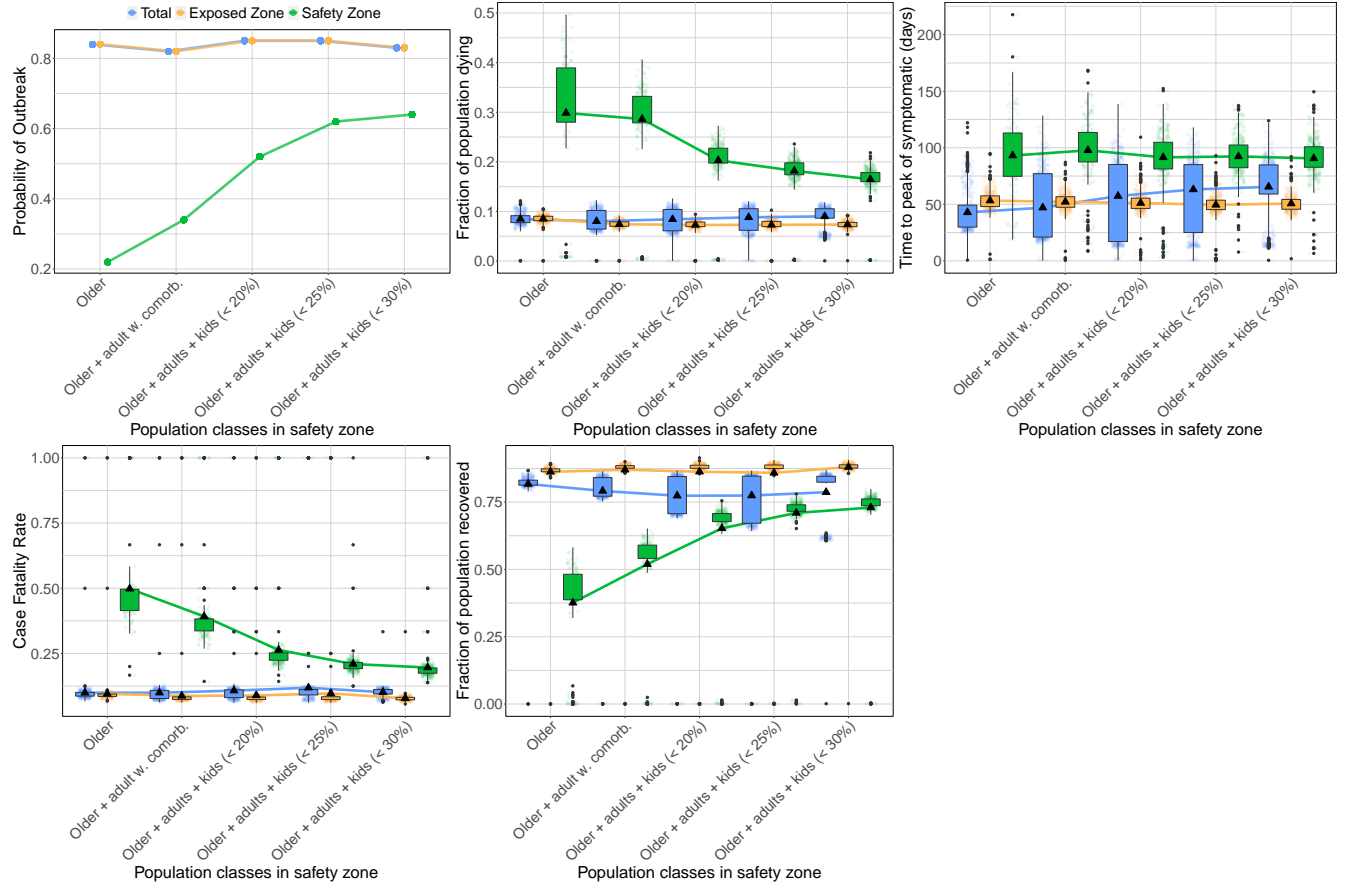


Figure 9: **Population moving to the safety zone.** Probability of an outbreak (top left), fraction of the population dying (top middle), time until peak symptomatic cases (top right), IFR (bottom left), and fraction of the population that recovers (bottom middle) as a function of the safety zone allocation scenario (see Table 1). All figures consider the scenario with 2 contacts in the buffer per person in the safety zone per week.

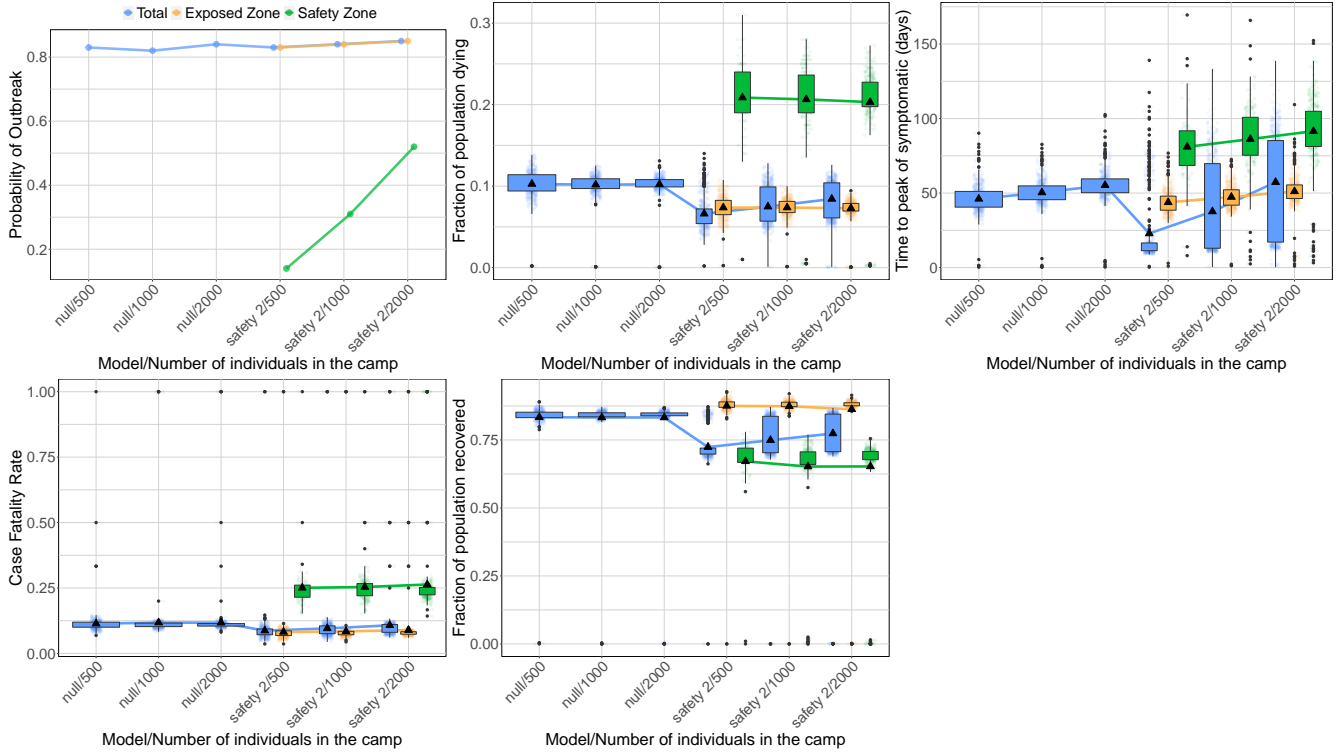


Figure 10: **Efficacy of the safety zone for different population sizes.** Probability of an outbreak (top left), fraction of the population dying (top middle), time until peak symptomatic cases (top right), IFR (bottom left), and fraction of the population that recovers (bottom middle) as a function of the total population size. The figures consider scenarios with no interventions (null), and with a safety zone comprising 20% of the camp's population with 2 contacts in the buffer zone per person in the safety zone per week (safety 2).

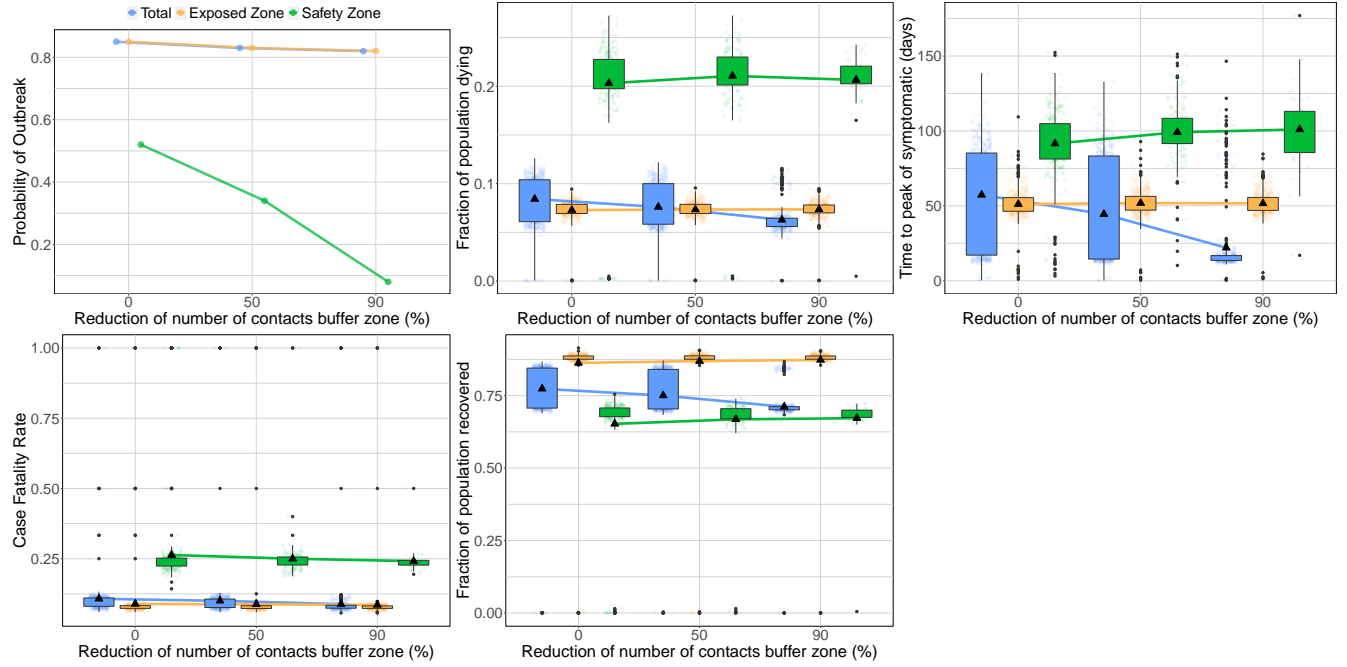


Figure 11: **Lockdown of the safety zone.** Probability of an outbreak (top left), fraction of the population dying (top middle), time until peak symptomatic cases (top right), IFR (bottom left), and fraction of the population that recovers (bottom middle) as a function of the reduction in the number of contacts permitted in the buffer zone from a baseline of 2 per person in the safety zone per week. All figures consider the scenario in which 20% of the camp's population is allocated to the safety zone.

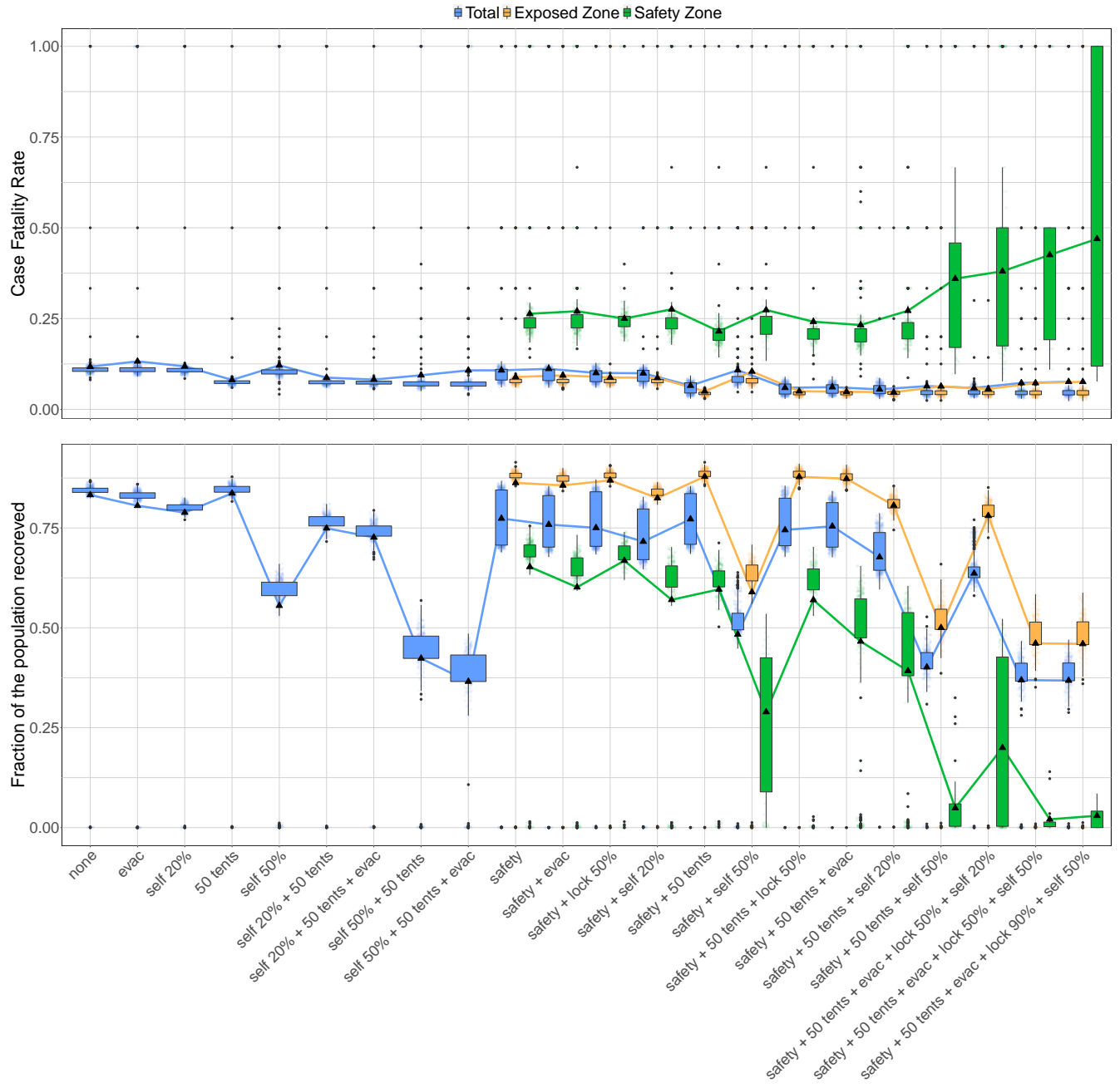


Figure 12: **Combined interventions.** IFR (top), and fraction of the population that recovers (bottom) for different combinations of interventions. Evac = evacuation of severely symptomatic, self = self-distancing, tents = number of available self-isolation tents, safety = safety zone, lock = lockdown of the buffer zone. For combinations of interventions including a safety zone, we distinguish between the population living in the green zone, in the orange zone and the whole population. The increase in the IFR for the green zone is explained by the discretization of the possible values that the IFR can take when the number of cases is very low (see Supplementary Table 2).

Intervention	<20 cases	Total	% of total
safety	16	270	5.9
safety + evac	20	249	8
safety + lock 50%	5	171	2.9
safety + self 20%	19	188	10
safety + 50 tents	11	240	4.6
safety + self 50%	14	64	22
safety + 50 tents + lock 50%	14	154	9.1
safety + 50 tents + evac	33	239	14
safety + 50 tents + self 20%	31	144	22
safety + 50 tents + self 50%	25	38	66
safety + 50 tents + evac + lock 50% + self 20%	53	110	48
safety + 50 tents + evac + lock 50% + self 50%	18	20	90
safety + 50 tents + evac + lock 90% + self 50%	6	8	75

Table 2: **Efficacy of the safety zone in combination with other interventions.** <20 cases = number of outbreaks in the green zone with fewer than 20 cases recorded. Total = total number of simulations where an outbreak in the green zone occurs (at least one death). % of total = percent of outbreaks where fewer than 20 cases are recorded. N = 500 simulations for each combination of interventions. For the most effective combinations, the majority of simulations where an outbreak occurs in the green zone see fewer than 20 cases. In these simulations, the discretization of the possible values that the IFR can take explains its apparently anomalous increase in Fig. 12.

References

- [1] Xi He, Eric HY Lau, Peng Wu, Xilong Deng, Jian Wang, Xinxin Hao, Yiu Chung Lau, Jessica Y Wong, Yujuan Guan, Xinghua Tan, et al. Temporal dynamics in viral shedding and transmissibility of COVID-19. *Nature medicine*, 26(5):672–675, 2020.
- [2] Peter Ashcroft, Jana S. Huisman, Sonja Lehtinen, Judith A. Bouman, Christian L. Althaus, Roland R. Regoes, and Sebastian Bonhoeffer. COVID-19 infectivity profile correction. *arXiv:2007.06602 [q-bio, stat]*, July 2020. arXiv: 2007.06602.
- [3] Jennifer Harcourt, Azaibi Tamin, Xiaoyan Lu, Shifaq Kamili, Senthil K Sakthivel, Janna Murray, Krista Queen, Ying Tao, Clinton R Paden, Jing Zhang, et al. Severe acute respiratory syndrome coronavirus 2 from patient with coronavirus disease, United States. *Emerging infectious diseases*, 26(6):1266, 2020.
- [4] Dawei Wang, Bo Hu, Chang Hu, Fangfang Zhu, Xing Liu, Jing Zhang, Binbin Wang, Hui Xiang, Zhenshun Cheng, Yong Xiong, et al. Clinical characteristics of 138 hospitalized patients with 2019 novel coronavirus-infected pneumonia in wuhan, china. *Jama*, 323(11):1061–1069, 2020.
- [5] Jeroen J.A. van Kampen, David A.M.C. van de Vijver, Pieter L.A. Fraaij, Bart L. Haagmans, Mart M. Lamers, Nisreen Okba, Johannes P.C. van den Akker, Henrik Endeman, Diederik A.M.P.J. Gommers, Jan J. Cornelissen, Rogier A.S. Hoek, Menno M. van der Eerden, Dennis A. Hesselink, Herold J. Metselaar, Annelies Verbon, Jurriaan E.M. de Steenwinkel, Georgina I. Aron, Eric C.M. van Gorp, Sander van Boheemen, Jolanda C. Voermans, Charles A.B. Boucher, Richard Molenkamp, Marion P.G. Koopmans, Corine Geurtsvankessel, and Annemiek A. van der Eijk. Shedding of infectious virus in hospitalized patients with coronavirus disease-2019 (COVID-19): duration and key determinants. *medRxiv*, page 2020.06.08.20125310, January 2020.
- [6] Assistance Coordinator Unit. The Syrian IDP camps monitoring study - Northern Syria camps - Humanitarian Data Exchange. url: <https://data.humdata.org/dataset/idp-camps-monitoring-november-of-2018>.
- [7] Shannon Doocy, Emily Lyles, Timothy Roberton, Laila Akhu-Zaheya, Arwa Oweis, and Gilbert Burnham. Prevalence and care-seeking for chronic diseases among Syrian refugees in Jordan. *BMC Public Health*, 15(1):1097, October 2015.
- [8] Shannon Doocy, Emily Lyles, Baptiste Hanquart, Michael Woodman, and The LHAS Study Team. Prevalence, care-seeking, and health service utilization for non-communicable diseases among Syrian refugees and host communities in Lebanon. *Conflict and Health*, 10(1):21, October 2016.
- [9] Yuanyuan Dong, Xi Mo, Yabin Hu, Xin Qi, Fang Jiang, Zhongyi Jiang, and Shilu Tong. Epidemiological characteristics of 2143 pediatric patients with 2019 coronavirus disease in china. *Pediatrics*, 2020.
- [10] Nancy Chow, Katherine Fleming-Dutra, Ryan Gierke, Aron Hall, Michelle Hughes, Tamara Pilishvili, Matthew Ritchey, et al. Preliminary estimates of the prevalence of selected underlying health conditions among patients with coronavirus disease 2019 in USA, february 12–march 28, 2020. *Morbidity and Mortality Weekly Report*, 69(13):382, 2020.
- [11] O. Diekmann, Hans Heesterbeek, and Tom Britton. *Mathematical tools for understanding infectious diseases dynamics*. Princeton series in theoretical and computational biology. Princeton University Press, Princeton, 2013.
- [12] Sydney Philipps, Dan Rossi, Rachel Von Arb, and Alex Capaldi. Mathematical models of infectious diseases: Two-strain infections in metapopulations, July 2011.
- [13] Marino Gatto, Enrico Bertuzzo, Lorenzo Mari, Stefano Miccoli, Luca Carraro, Renato Casagrandi, and Andrea Rinaldo. Spread and dynamics of the COVID-19 epidemic in Italy: Effects of emergency containment measures. *Proceedings of the National Academy of Sciences*, 117(19):10484–10491, May 2020.
- [14] J.M Heffernan, R.J Smith, and L.M Wahl. Perspectives on the basic reproductive ratio. *Journal of the Royal Society Interface*, 2(4):281–293, sep 2005.